ARTICLE

Pore-size distribution of a compacted silty soil after compaction, saturation, and loading

M. Oualmakran, B.C.N. Mercatoris, and B. François

Abstract: Soil microstructure is an important feature that controls soil behaviour at the macroscale. This microstructure depends on the sample preparation method and evolves during saturation and loading. This paper investigates the effects of compaction water content, drying techniques adopted prior to performing porosimetry, saturation and loading on the evolution of the microstructure of a silty soil. Mercury intrusion porosimetry is used to obtain the pore-size distribution at different states of soil presenting single and double porosity. It is observed that in presence of aggregates (obtained from a compaction on the dry side of optimum), the bimodal pore-size distribution is not significantly affected by the saturation process at zero stress. This feature of behaviour is quite specific to low plasticity silty soil. Conversely, loading under saturated conditions has a more significant effect on the pore-size distribution. This bimodal distribution converges into a single mode of pore size when the stress is significantly greater than the apparent preconsolidation pressure. The observed experimental results are interpreted in the light of pore-size distribution evolution during saturation and loading.

Key words: microstructure, mercury intrusion porosimetry, compaction, structured soil, destructuration.

Résumé : La microstructure d'un sol est un paramètre important qui conditionne son comportement macroscopique global. Cette microstructure dépend du mode de préparation des échantillons et évolue durant les phases de saturation et de chargement. Cet article étudie l'effet de la teneur en eau de compactage, des techniques de séchage nécessaire à la réalisation des porosimétries, de la saturation et du chargement mécanique sur l'évolution de la microstructure d'un sol limoneux. La technique de la porosimétrie par intrusion de mercure est utilisée pour obtenir la distribution de la taille des pores pour différents états du sol présentant des porosités simples ou doubles. On observe qu'en présence d'agrégats (obtenus en compactant le sol du côté sec de l'optimum), la distribution bimodale de la taille des pores n'est pas modifiée significativement durant la phase de saturation sous contrainte nulle. Au contraire, le chargement mécanique effectué en conditions saturées modifie beaucoup plus significativement la distribution de la taille des pores. Ce comportement est assez spécifique aux limons à faible plasticité. Cette distribution bimodale converge vers un mode unique de taille des pores quand le chargement vertical dépasse significativement la contrainte de préconsolidation apparente. Les résultats expérimentaux sont interprétés sur base de l'évolution de la distribution de la taille des pores durant la saturation et le chargement.

Mots-clés : microstructure, porosimétrie au mercure, compactage, sol structuré, déstructuration.

Introduction

Structured soils are involved in many applications in geotechnical engineering. It concerns natural soils for which the structure can arise from sedimentary depositions or from chemical bondings or dissolutions (Leroueil and Vaughan 1990; Liyanapathirana et al. 2005). Also, earthen constructions are generally made of structured soils due to their particular modes of construction by soil compaction (Alonso et al. 2010).

The term "structure" gathers the "fabric" and "bonding" concepts. The fabric concerns the arrangement of particles and voids while the bonding refers to interparticles forces acting to connect particles (Cotecchia and Chandler 1997; Mitchell 1976).

In the present study, the "microstructure" must be understood as the "fabric" in the sense that we will exclusively focus on the arrangement of particles and particularly the distribution of pore sizes.

There are different experimental techniques to evidence the soil microstructure (Romero and Simms 2008). Amongst them, mercury intrusion porosimetry (MIP) aims at characterizing the multiple porosity of soil through the determination of the pore-size distribution (PSD). MIP is based on the principle that nonwetting fluid does not enter a porous medium unless a pressure is applied (Delage and Lefebvre 1984). The soil sample is submerged into mercury and the applied pressure can be related to the size of pore. The pressure increases progressively allowing thinner pores to be filled with mercury. The volume of mercury intruded in function of the pressure gives the PSD. Depending on the limit of the injected pressure, very small pores (nanoscale) are not intruded, which makes the technique inappropriate to study intraparticle (interplatelet) pore space of clay particles. This size of pore will not be considered in the present study. The PSD differential put forward the characteristic pore sizes by the appearance of peaks in the curve corresponding to pore size with high frequency of occurrence.

Romero and Simms (2008) discuss the different advantages and drawbacks of the technique. Despite some limitations, MIP re-

M. Oualmakran and B. François. Building Architecture and Town Planning Department (BATir), Université Libre de Bruxelles, Avenue F.D. Roosevelt 50, CP 194/2, 1050 Brussels, Belgium.
B.C.N. Mercatoris. Biosystem Engineering Department (BIOSE), Gembloux Agro-Bio Tech, Université de Liège, Passage des Déportés 2, 5030 Gembloux, Belgium.
Corresponding author: B. François (email: Bertrand.Francois@ulb.ac.be).

mains a reliable technique to study the microstructure of fine-grained soils through the distribution of the size of their voids.

In the most general conditions, three main classes of pores can be evidenced: intraparticle porosity, intraaggregate porosity, and interaggregate porosity (Monroy et al. 2010). Let us note that the intraparticle porosity concerns nanoscale that is not always observable with conventional MIP. In the following, that intraparticle porosity will be omitted and considered as the solid phase. In presence of the two other pore categories, the soil can be qualified as "structured" in the sense that the pores inside and outside the aggregates exhibit a significant difference of sizes. In contrast, an unstructured soil shows only a single distribution, characterized by one characteristic pore size around the particle (Delage et al. 1996; Hattab et al. 2015).

The presence of structure in remoulded soils is a function of the compaction conditions. A soil compacted in dryer conditions than the optimum water content presents aggregates contrary to the wet side of optimum (Delage et al. 1996; Watabe et al. 2000; Monroy et al. 2007, 2010; Alonso et al. 2013). At low water content, capillary effect tends to link particles together during the compaction. Consequently, aggregates are formed with the water that is enclosed inside the aggregate and air occupies the large voids between aggregates. On the contrary, when water content is high, water pushes the grains apart during compaction and produces a dispersed structure of clay platelets.

Soil structure affects the hydromechanical behaviour of the soil (Delage and Lefebvre 1984; Monroy et al. 2007). This difference of behaviour can be brought out by different geomechanical laboratory tests. In particular, in œdometric compression tests, unstructured soil undergoes elastic strain until a threshold value called preconsolidation stress "σ_{vp}". This is commonly considered as the highest stress sustained by the soil and can be related to soil density (Burland et al. 1996; Monroy et al. 2010). Beyond this threshold, the stress path follows the "intrinsic compression line" (ICL), which is a straight line governed by the compression index C_c. Structured soil can go over the ICL and reaches an area unreachable for the unstructured soil. Its apparent preconsolidation stress is higher. This preconsolidation stress is called "apparent" because it arises from the soil structure that can disappear due to mechanical or chemical "destructuration" and is not only related to the highest stress sustained by the soil. Therefore, the effect of structure can lead to an overconsolidation state (Leroueil and Vaughan 1990; Hattab et al. 2013). The compression index is not clearly defined, but it is higher than for unstructured soil and decreases with increasing stress (Delage and Lefebvre 1984; Graham and Li 1985).

This enhancement of the yield limit is due to the structure effect that decreases after the threshold from which significant structural breakdown begins. This process is called "destructuration" and is an important feature of the mechanical behaviour of structured soils. The alteration of the structure is progressive and important strain is required to remove the structure (Leroueil and Vaughan 1990). After complete removal of the structure, the stress path follows a "normal compression line" (NCL) assumed to be a straight line (Monroy et al. 2010). The NCL can coincide with the ICL or be parallel. In this case, further strain can be required to obtain similar fabric and join the ICL (Burland et al. 1996; Yang et al. 2014).

For soils compacted on the dry side of optimum, at a same water content, but in denser condition, the macroporosity and its characteristic diameter is much smaller (Birle 2012; Airò Farulla and Rosone 2012). This difference appears only in the larger interaggregate pores (Romero et al. 1999; Li and Zhang 2009; Sivakumar et al. 2006; Thom et al. 2007; Nowamooz and Masrouri 2010; Birle 2012). The intraaggregate pores are also affected, but to a lesser extent (Thom et al. 2007).

With increasing water content of compaction, the capillary effect decreases and aggregates become softer. Thereby the larger interaggregate pores diminish and the percentage of intraaggregate pores increases (Thom et al. 2007; Birle 2012; Tarantino and De Col 2008).

During saturation, the smaller pores are the first to be saturated because of the capillary effect (Delage et al. 1996). The aggregates swell and the microstructural expansion progressively invades the macropores space (Romero and Simms 2008). Consequently, an increase of the microporosity is observed with a decrease of the macroporosity (Monroy et al. 2010) and the bimodal distribution evolves to an new dominant single mode (Airò Farulla and Rosone 2012; Romero and Simms 2008; Koliji et al. 2010). Also, it is clear that the transition from a bimodal PSD toward a unimodal distribution strongly depends on the swelling capacity of the clay mineral. For a swelling clay at a state close to saturation, the pore space is homogeneous as the aggregates swell and eventually occupy the entire interaggregate void space while a low activity clay or a silty soil would not exhibit such a significant destructuration upon saturation.

Loading mainly affects the larger interaggregate porosity without remarkably changing inside the aggregates (Delage and Lefebvre 1984; Griffiths and Joshi 1989; Lapierre et al. 1990; Al-Mukhtar et al. 1996; Monroy et al. 2007; Romero and Simms 2008; Koliji et al. 2008; Monroy et al. 2010; Hammad et al. 2013). The largest interaggregates pores are the most collapsible and therefore the first affected by the loading, followed by progressively smaller and smaller pores. In this sense, as the compression index evolves during loading, it can be related to the largest class of pores (Delage and Lefebvre 1984; Kochmanova and Tanaka 2011).

In that framework, the goal of this study is to analyze the evolution of the microstructure during saturation and mechanical loading of a silty soil prepared by compaction at different water contents, but at the same dry density.

The difference in macroscopic behaviour is brought out by œdometric tests. The microstructure is investigated at different states of loading with MIP to relate the macroscopic and the microscopic behaviour. The impact of different drying techniques adopted prior to performing MIP is discussed.

Materials and experimental procedures

Soil
The grain-size distribution (Fig. 1) presents a clayey fraction of 23%, 67% of silt, and 10% of sand. The liquid limit is 28.4% and the plastic index is 8.8%. It is a clayey silt according to the Unified Soil Classification System (USCS) classification (CL-ML; ASTM (2006) standard D2487-06). The specific gravity of solid particles is 2.69. The modified optimum Proctor was obtained at a water content of 15% with a dry density of 18.1 kN/m³ (Fig. 2).

Sample preparation for œdometric test
To study the effect of the compaction water content on the obtained soil structure, samples were dynamically compacted at two different water contents, on the dry and wet sides of optimum. On the one hand, for the dry side of optimum, a water content of 12% was imposed for the compaction. The soil is termed "SD" (for "structured dry"). On the other hand, the samples at the wet side of optimum were obtained from a compaction at a water content of 20%. It is termed "UW" (for "unstructured wet"). All the samples were compacted at the same dry density of 16 kN/m³, below the Proctor curve, to have a low preconsolidation stress and to enlarge the range of stress upon which soil structure degradation can occur. This dry density corresponds to a void ratio of 0.66.

The soil was prepared by first mixing a quantity of dry soil with distilled water to reach the considered water content. This wet soil was stored at least 24 h in a humidity-controlled room for homogenization. All the samples were compacted at the same dry density to provide the same initial void ratio for all the tests. The samples were dynamically compacted in a mould of 50 mm diam-

Fig. 1. Grain-size distribution of studied silty soil.
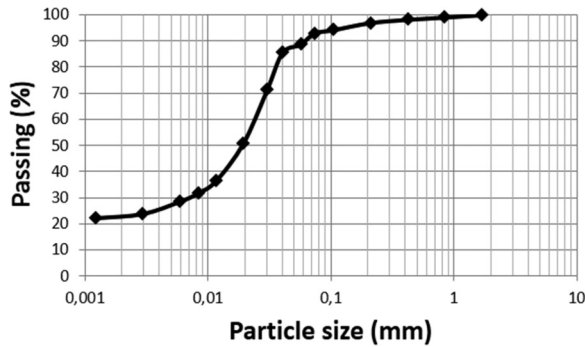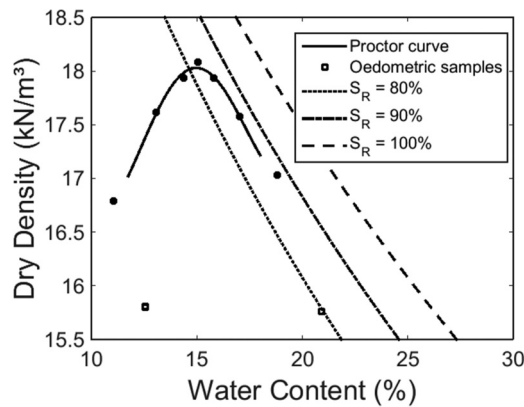

Fig. 2. Modified Proctor curve and conditions of compacted samples (on dry and wet sides of optimum at relatively low dry density). S_r, degree of saturation.

Fig. 3. Œdometric compression test on unstructured (compacted on wet side of optimum — blue squares) and structured (compacted on dry side of optimum — red circles) soils. Test was performed three times upon each condition. Curve is the average behaviour. [Colour online.]
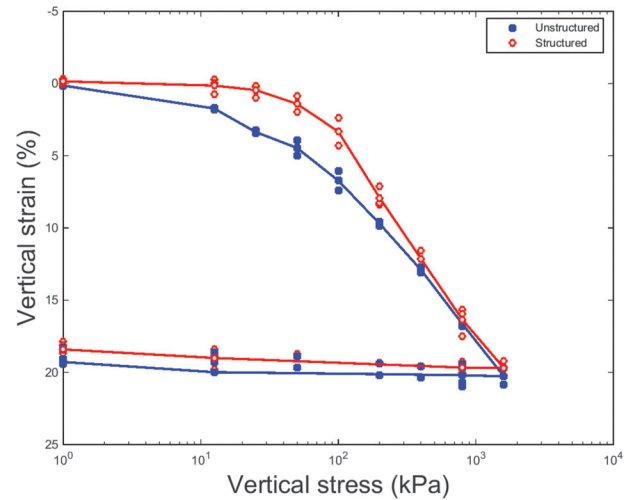

Fig. 4. Difference of strain between structured and unstructured soils.

eter by tamping the mass of wet soil corresponding to the target density. The samples were compacted in one layer. The target volume is ensured by a piston equipped with a stop. This dry density corresponds to a void ratio of 0.66 and a degree of saturation of 93% and 47%, respectively, for UW and SD. The œdometric samples are 16 ± 0.5 mm in height. Then, the samples were put in the œdometric cell and immersed into distilled water for water saturation under zero external stress (the samples were not submitted to any vertical stress during saturation except the weight of the porous stone and the top cap (±1 kPa)). The saturation step is at least 72 h long.

The soil samples were then incrementally charged under saturated conditions. The loading began at 12.5 kPa and increased until 1600 kPa by doubling the load at each step. Each loading step lasted 24 h to permit the consolidation to occur.

Sample preparation for MIP

To determine the PSD of soil through MIP, soil fragments of around 1 cm³ were taken from samples after different steps of the process: after compaction, after saturation, after loading at 100 kPa under saturated conditions, and after loading at 1600 kPa under saturated conditions.

First, those soil fragments needed to be dried. Several drying techniques exist and they are not all equivalent in regards with their impact on the microstructure. It is indeed known that the microstructure can be altered by drying (Simms and Yanful 2002). The purpose is then to minimize the soil degradation during drying and in particular to avoid the shrinkage of the microstructure (Delage and Pellerin 1984; Lawrence et al. 1979).

In this study, three drying techniques prior to MIP were investigated to determine their effects on the obtained PSDs.
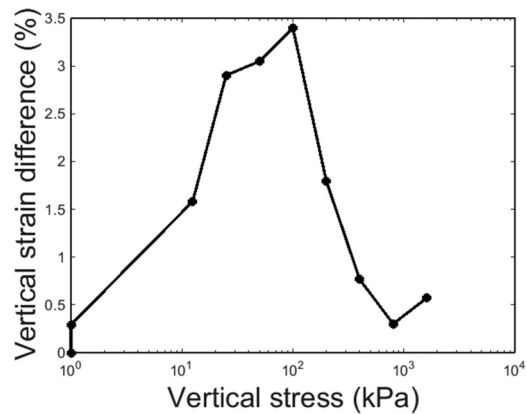
1. The freeze-drying technique permits to dehydrate the sample by sublimation. Detailed accounts of freeze-drying techniques have been given by Ahmed et al. (1974); Delage et al. (1982); Delage and Pellerin (1984); Penumadu and Dean (2000). This technique is the most used in the framework of MIP and aims at maintaining the microstructure as undisturbed as possible (Tovey and Wong 1973; Tessier and Berrier 1978) because no air–water capillary menisci are formed during drying (Delage et al. 1996).

2. Commonly in the laboratory, the soil is dried in an oven at 105 °C during 24 h. It is expected that this technique may slightly disturb the microstructure because of the shrinkage that occurs during drying or by dilation due to the temperature.

3. To avoid the disturbing effect of high-temperature drying, a third technique consists in drying the soil in an oven at a lower temperature (40 °C). The sample stays in the oven until no mass change is observed (generally 72 h).

Sample properties

Names are given to samples according to the water content of compaction, the state of saturation and loading, the drying technique, and the number of the sample. A glossary is presented below.

• P: porosimetry
• UW/SD: wetter/dryer conditions of compaction than the optimum water content.

Table 1. Summary of tested conditions for mercury intrusion porosimetry (MIP) with naming convention of each condition.

	Phase	Freeze-dried	Oven at 40 °C	Oven at 100 °C
Dry side of optimum	As compacted	PSDACFD (3)	PSDACOL (2)	PSDACOH (4)
	After saturation	PSDSATFD (2)	—	—
	After loading at 100 kPa	PSD100FD (4)	—	—
	After loading at 1600 kPa	PSD1600FD (2)	—	—
Wet side of optimum	As compacted	PUWACFD (4)	PUWACOH (2)	PUWACOH (2)
	After saturation	PUWSATFD (4)	—	—
	After loading at 100 kPa	PUW100FD (2)	—	—
	After loading at 1600 kPa	PUW1600FD (2)	—	—

Note: Number between brackets refers to the number of repetitions of the same tests. A total of 33 MIP were performed.

- AC/SAT/100/1600: as-compacted/saturated/100 kPa/1600 kPa. Soil tested before or after saturation, or after being submitted to a vertical stress of 100 or 1600 kPa in the œdometer under saturated conditions.
- FD/OH/OL: drying techniques: freeze-dried/oven at high temperature (105 °C)/oven at low temperature (40 °C).
- 1/2/3/4: number of the sample.

As an example, the sample "PUW100FD2" is the second sample compacted on the wet side of optimum, freeze-dried after a loading of 100 kPa.

Œdometric compression test results

The œdometric compression test brings out the different compressibility behaviour of the two soils compacted upon two different water contents (dry (SD) and wet (UW) sides of optimum). Each test has been performed three times. Figure 3 reports the results. The curves represent the averaged behaviour amongst the three tests.

The elastic behaviour of both soils is similar. The swelling indexes C_s determined on the unloading part of the curves are 0.0051 and 0.0067, respectively, for UW and SD samples, which are very close to each other.

An important effect of structure is the increase of the apparent preconsolidation pressure σ_{vp}, which is equal to 40 kPa for the UW and reaches 70 kPa for SD. This preconsolidation pressure has been obtained by Casagrande construction (Casagrande 1936).

When the stress exceeds the σ_{vp} of the SD (around 100 kPa), both curves tend to converge. During the last increment of loading, between 800 and 1600 kPa, the strain and the compressibility are very similar for both soils.

Figure 4 expresses the difference between the vertical strain reached by each soil during loading. In a first phase, the vertical strain difference increases due to the progressive plasticity that develops in the unstructured soil while the structured soil remains elastic. Then, in a second phase, when the apparent preconsolidation pressure of the structured soil is exceeded, this difference decreases due to the destructuration of the structured soil.

MIP results

The œdometric compression tests show different behaviour between soils compacted on dry (SD) and wet (UW) sides of optimum. The MIP allows to evidence if this difference in the macroscopic behaviour results from a change of the soil structure at the microscopic scale.

In total, 33 MIP tests were carried out under different conditions, as summarized in Table 1. Test upon each condition was repeated several times to check the reproducibility of the results. MIP of samples compacted on dry and wet sides of optimum were performed just after compaction, after saturation, and after oedometric loading at 100 and 1600 kPa under saturated conditions. For the samples tested just after compaction, three techniques of drying adopted prior to MIP were investigated. It was observed that the freeze-drying was the least disturbing method in terms of

void ratio evolution. This point will be further discussed in detail in section titled "Effect of drying techniques prior to porosimetry". Consequently, solely this freeze-drying technique was applied for the other conditions.

Figure 5 reports all the obtained PSDs upon those different conditions. The reproducibility is very good, except a slight discrepancy for the unstructured soils just after saturation and for the structured soil at 100 kPa of loading. Those small variabilities can be explained because the unstructured soil after saturation is very soft and may be partially disturbed during handling while the vertical stress of 100 kPa is around the apparent preconsolidation pressure of the structure soil, which makes the soil structure very sensitive to the stress level (after the apparent preconsolidation pressure, the structure is progressively deteriorated). At the end, from the series of obtained curves, the most representative test results were presented and discussed.

In the following, the curves are analyzed in terms of micro and macrovoids. The derivative of the PSD is taken to represent the frequency of appearance of each pore size. A bimodal curve is classically attributed to two distinct characteristic pore sizes. The first peak represents micropores and is expressed by the subscript μ while the second peak is macropores expressed by the subscript M.

The pore diameter (D) of each peak is also recorded. The minimum between the two peaks is considered as the boundary between microporosity and macroporosity. This limit between microporosity and macroporosity is specific to each soil and is not related to any standard of pore-size separation. Let us note also that nanopores is out of our scale of interest because the maximum mercury pressure is of 33 000 psi (1 psi = 6.895 kPa), corresponding to a minimum diameter of intruded pores of 5.6 nm.

In the case of unimodal PSD, all the voids are associated to microvoids, the pores out of the main mode of the PSD on both ends of the distribution are disregarded. Consequently, the microvoid ratio is slightly different from the total void ratio.

The values of void ratios and characteristic diameters for each condition are reported in Table 2.

Effect of drying techniques prior to porosimetry

Concerning the effect of drying techniques adopted prior to porosimetry, Fig. 6 compares the differential PSD of both soils dried by freeze-drying or by warming at low and high temperatures. The characteristic pore diameter of the UW seems globally unaffected by the drying process, staying around 2 μm. Nevertheless, the void ratio relatively unaffected by the freeze-drying technique (e = 0.50) is significantly reduced during drying in the oven, at both moderated and high temperatures (e = 0.36 and 0.34, respectively). The warming along drying produces a closure of the larger voids (bigger than 2 μm), as shown in Fig. 6, leading to a drastic decrease of void ratio.

The effects of the drying technique on the SD appear less sensitive in terms of total void ratio: the void ratio of the freeze-dried sample is around 0.54 such as the sample dried in the oven at high temperature while it decreases until 0.50 for the sample dried in the oven at low temperature. However, Fig. 7 shows that the dis-

Fig. 5. Pore-size distributions (PSD) of the 33 tests under different conditions. Left: samples compacted on dry side of optimum; right: samples compacted on wet side of optimum. Naming conventions are reported in Table 1. [Colour online.]
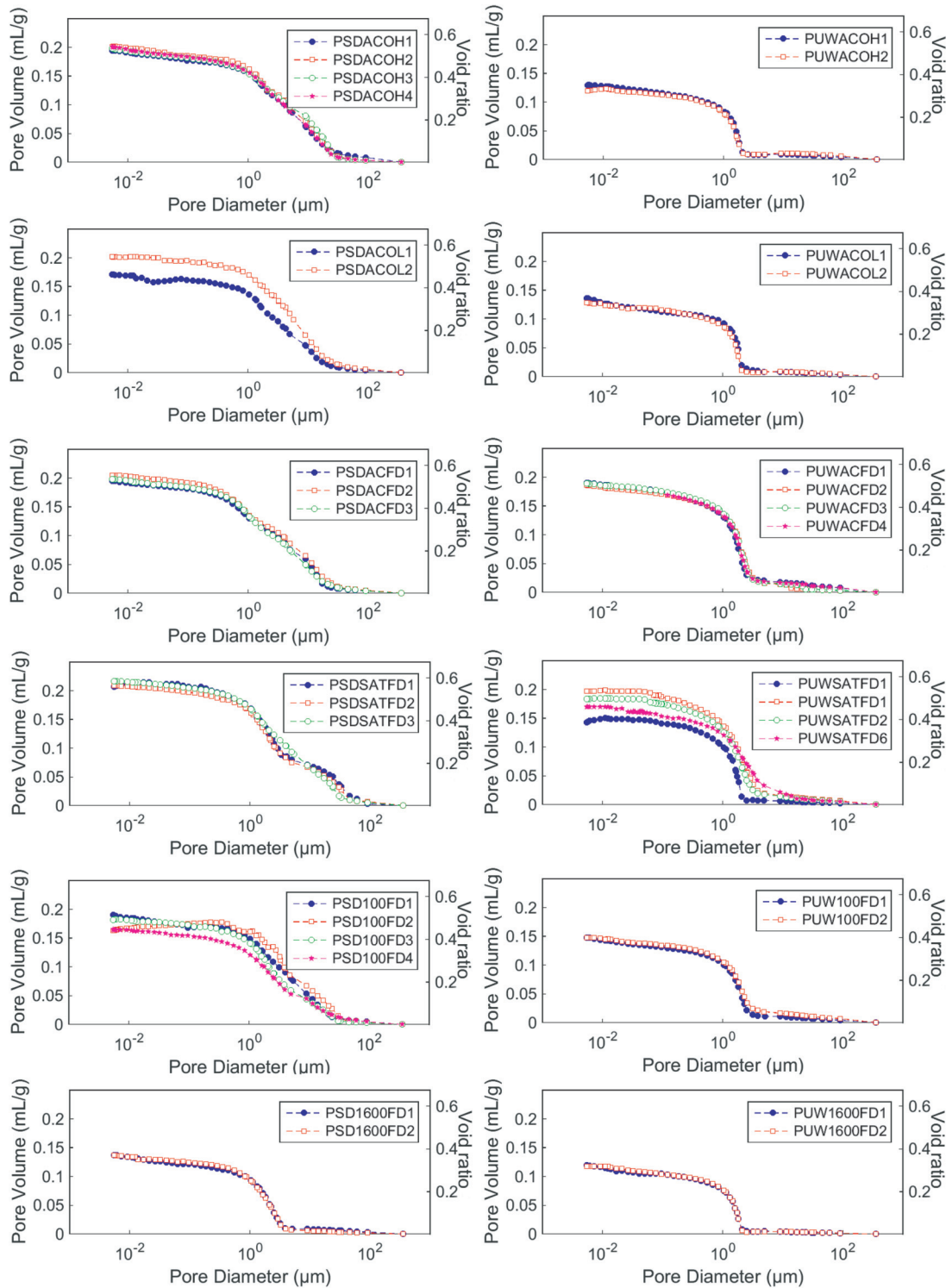
tribution of micropores is affected by temperature of drying. Warming dilates the micropores, the diameter increasing from 0.81 μm for the freeze-dried samples to 1.80 and 1.85 μm for the drying in the oven at 40 and 105 °C, respectively.

As freeze-drying technique seems the less disturbing method in terms of total void ratio, we can expect that it is the least disturbing drying technique. Consequently, this technique was adopted for all the other samples.

Soil structure

Figure 8 compares the differential PSDs of soils compacted on dry and wet sides of optimum, after freeze-drying of as-compacted samples. This first comparison clearly evidences the difference of PSD between soils compacted on the dry side of optimum (i.e., SD, structured soil) and on wet side of optimum (i.e., UW, unstructured soil). UW samples exhibit a unimodal PSD while SD specimens clearly present a bimodal PSD.

Published by NRC Research Press

Table 2. Interpretation of pore-size distribution (PSD) in terms of total void ratio (e), diameter of micropores (D_μ), diameter of macropores (D_M), microvoid ratio (e_μ), and macrovoid ratio (e_M).

Sample	e	D_μ (μm)	D_M (μm)	e_μ	e_M	$\dfrac{e_\mu}{e}$	$\dfrac{e_M}{e}$
PSDACOH	0.54	1.80	9.06	0.26	0.28	0.48	0.52
PSDACOL	0.50	1.85	7.48	0.19	0.31	0.39	0.61
PSDACFD	0.54	0.81	9.33	0.25	0.29	0.46	0.54
PSDSATFD	0.58	2.01	29.13	0.40	0.17	0.70	0.30
PSD100FD	0.48	2.21	17.20	0.31	0.18	0.63	0.37
PSD1600FD	0.37	2.69	—	0.35	—	0.95	—
PUWACOH	0.34	1.70	—	0.32	—	0.93	—
PUWACOL	0.36	1.79	—	0.34	—	0.94	—
PUWACFD	0.50	2.02	—	0.46	—	0.92	—
PUWSATFD	0.52	2.13	—	0.47	—	0.91	—
PUW100FD	0.40	2.10	—	0.36	—	0.91	—
PUW1600FD	0.32	1.74	—	0.31	—	0.96	—

Fig. 6. Differential PSD of as-compacted unstructured soil subjected to different drying techniques prior to performing mercury intrusion porosimetry (MIP). FD, freeze-dried; OL, oven at 40 °C; OH, oven at 105 °C. [Colour online.]

Fig. 7. Differential PSD of as-compacted structured soil submitted to different drying techniques prior to performing the MIP. FD, freeze-dried; OL, oven at 40 °C; OH, oven at 105 °C. [Colour online.]

Fig. 8. Differential PSD of as-compacted soil, after freeze-drying. Comparison of the effect of compaction water content. W, wet side of optimum; D, dry side of optimum. [Colour online.]
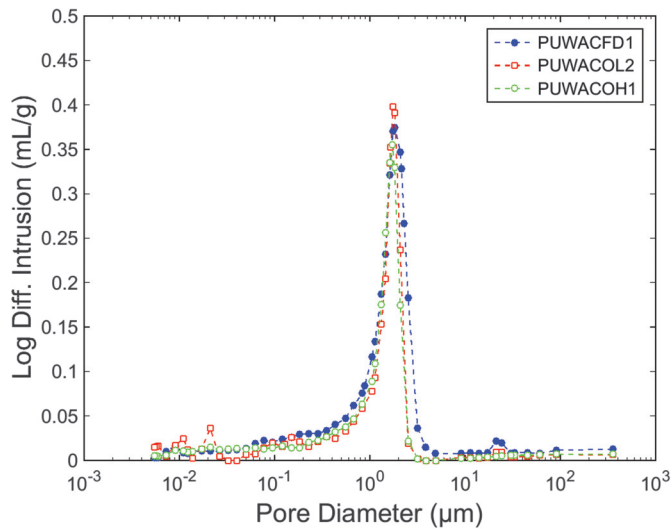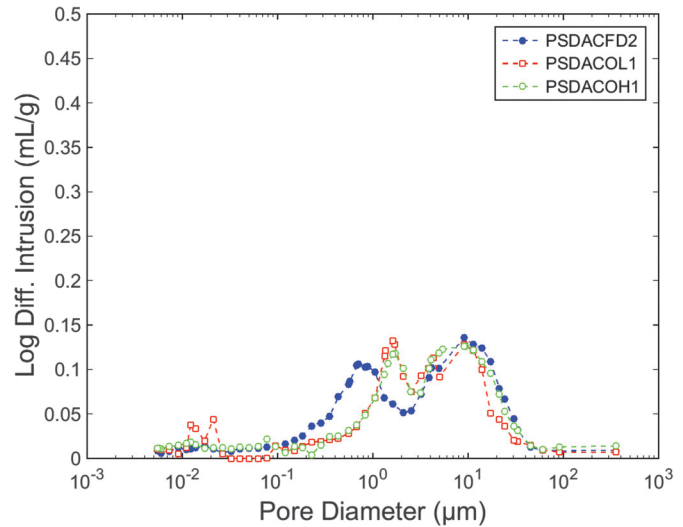

Figure 9 shows the evolution of the differential PSD of soils compacted on the wet side of optimum (UW samples) after compaction, after saturation, after loadings at 100 and 1600 kPa under saturated conditions. The unimodal curve is not highly affected neither by the saturation process upon zero stress nor by the loading. The peak stays around 2 μm, but the total void ratio evolves significantly.

During re-saturation, larger micropores appear without modifying the total porosity. The pore distribution extends up to 5 μm while it was limited to 3 μm in the as-compacted state. This change results from a merge of small voids (1–2 μm) unchanging the total void volume.
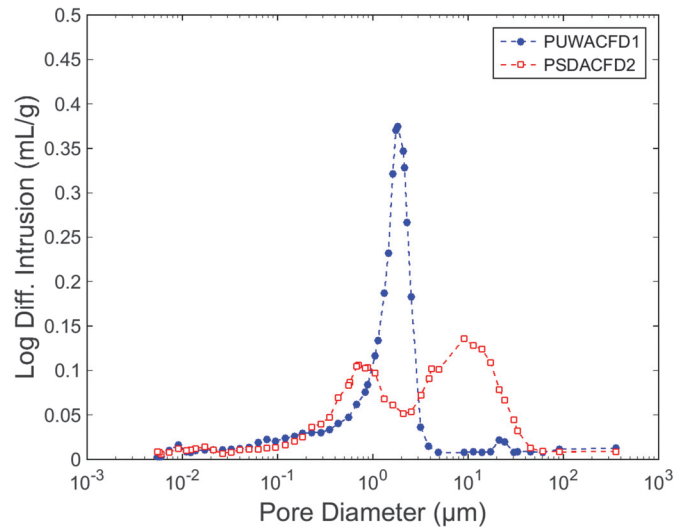
Upon loading, the void ratio decreases through the closure of the biggest micropores. The loading at 100 kPa closes pores larger than 3 μm, reducing the void ratio of 0.12. It corresponds to a vertical strain of 5% that is observed in the œdometric curve (Fig. 3). A higher stress provokes the closure of the coarser pores and no pores higher than 2 μm remain.

As far as soils compacted on the dry side of optimum is concerned (SD samples), Fig. 10 shows that the bimodal differential PSD evolves significantly during saturation and loading to finally becomes unimodal upon a vertical stress of 1600 kPa.

The saturation phase does not imply important swelling, but provokes a shift to the right of the differential PSD: the peak of micropores increases from 0.81 to 2.01 μm while the macropores peak passes from 9.33 to 29.13 μm. It appears that the saturation affects the PSD, but does not modify the macroscopic volume of the sample. The increase of pore sizes is compensated by the macropore volume decrease. This is probably due to the nonswelling character of the tested soil.

The loading provokes the closure of the macropores without affecting the micropores. These latter stay between 1.7 and 2.7 μm. The macropores peak reaches 17.2 upon 100 kPa and totally disappears upon 1600 kPa where the PSD becomes unimodal.

Interpretation

Water content at compaction affects the mechanical behaviour of the soil. The structured soil (compacted on the dry side of optimum, SD) presents a higher apparent vertical preconsolidation stress and then a higher compression index to converge to

Fig. 9. Evolution of differential PSD of unstructured soil during saturation and loading. Loading is performed upon saturated conditions. AC, as-compacted; SAT, after saturation; 100, after vertical load of 100 kPa; 1600, after vertical load of 1600 kPa. [Colour online.]
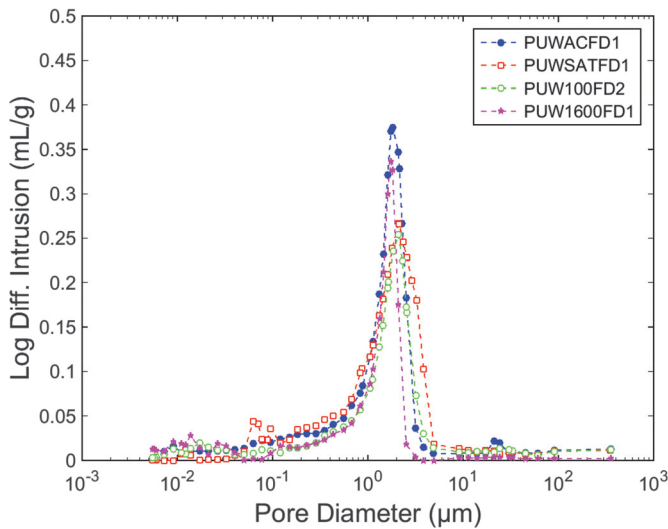
Fig. 10. Evolution of differential PSD of structured soil during saturation and loading. Loading is performed upon saturated conditions. AC, as-compacted; SAT, after saturation; 100, after vertical load of 100 kPa; 1600, after vertical load of 1600 kPa. [Colour online.]
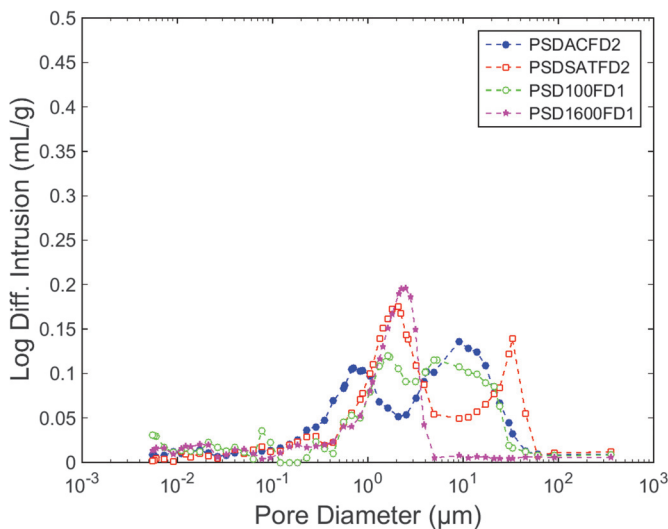

the curve of unstructured soil (compacted on wet side of optimum, UW).

This behaviour is symptomatic of the presence of structure. Interparticle bonds link particles inside aggregates and are responsible for the elastic domain increase. Plastic strain occurs with bonds breaking and SD soil becomes fully destructured after large compressive strains. This destructuration explains the convergence of SD and UW behaviour.

The PSD of the unstructured soil keeps its unimodal shape with a single class of pores upon saturation and loading (Fig. 9). The UW deformation affects mainly the biggest micropores. The addition of water rearranges the soil particles inducing a merge of the finest pores to create bigger voids, while the unimodal character of the curve is maintained. Throughout the loading, the coarsest class of pores is affected. The closure of the biggest pores narrows the peak to the finest pores.

Fig. 11. Differential PSD of soil compacted on dry side (D) and wet side (W) of optimum after a vertical loading of 1600 kPa under saturated conditions. [Colour online.]
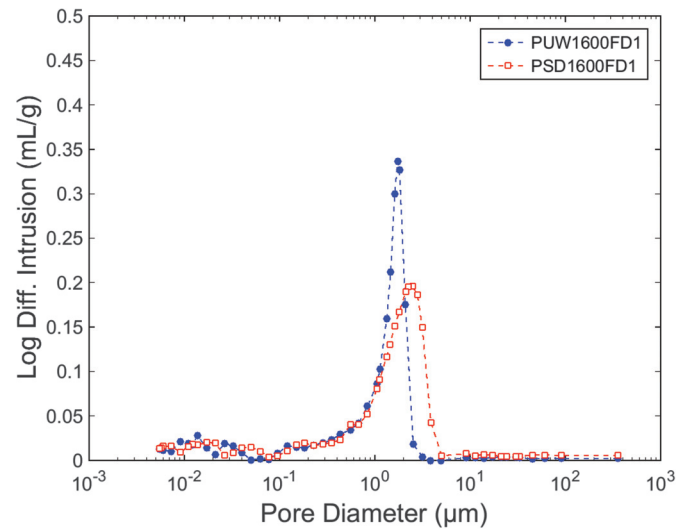
For structured soil, saturation upon zero stress provokes aggregates swelling and increases the micropores size and volume. This expansion induces an invasion of the macropores, reducing the interaggregates volume, and a rearrangement of the aggregates, merging the macropores and increasing their size (Fig. 10). The shape of the PSD is modified, but keeps a bimodal trend.

Upon loading under saturated conditions, aggregates crumble. The amount of microvoids is progressively reduced due to the crumbling of aggregates. The particles leaving the aggregates invade the interaggregates voids, leading to a reduction of the size of the interaggregates voids. This process creates intermediate pores and the double-porosity progressively vanishes. At 100 kPa, the PSD is quasi-unimodal even if a small distinction between micro and macropores persists. Progressively, the PSD becomes unimodal and covers a larger pore size range.

Even if the void ratio and the characteristic diameter of the SD and the UW are very similar after being loaded at 1600 kPa, Fig. 11 brings out a significant difference in the PSD. The UW soil presents a more marked peak than SD soil, which contains larger pores. Consequently, the destructuration induced by mechanical loading does not merge perfectly the two PSDs and the initial effect of compaction persists. The soil compacted on the dry side of optimum inherits the larger pores from the macropores of the as-compacted material, even if the bimodal characters of the curve disappears.

Conclusion

This study highlights the effects of the compaction conditions on the soil microstructure by comparing the PSD evolution upon saturation at zero stress and loading of a silty soil compacted under two different conditions: on the wet side of optimum and on the dry side of optimum. We observe peculiar evolutions of the microstructure characteristic of a low plasticity silty soil. First of all, the saturation process performed under zero stress does not significantly alter the PSD. The bimodal character of the PSD of soil compacted on the dry side of optimum is essentially maintained during saturation. This is linked to the stable (i.e., non-swelling) behaviour of silty particles during hydration. Then, during oedometric loading under saturated conditions, the bimodal distribution of the pores of structured soils tends towards a single mode of pores, the macropores being progressively closed while the mean size of the micropores are slightly increased. For the unstructured materials, the unimodal shape of PSD is main-

tained all along the loading process, the largest pores of this distribution being closed.

For the construction of earth structures (embankments, earth-fill dikes, industrial platforms), nonswelling silty materials are frequently used as an appropriate material because of its wide availability in the field and its relatively good mechanical property (by opposition to plastic clays). In that context, this study demonstrates that the saturation process has a limited impact on the soil structure. Also, the compaction on the dry side of optimum permits to increase the apparent preconsolidation pressure that may be of significant interest to limit the deformation of the earthfill structure upon loading. It is shown that this enhancement of the apparent preconsolidation pressure is maintained even after a full saturation of the material upon zero stress.

Acknowledgement

References

Ahmed, S., Lovell, C., and Diamond, S. 1974. Pore sizes and strength of compacted clay. Journal of the Geotechnical Engineering Division, ASCE, **100**(4): 407–425. doi:10.5703/1288284314552.

Airò Farulla, C., and Rosone, M. 2012. Microstructure characteristics of unsaturated compacted scaly clay. *In* Unsaturated soils: research and applications. *Edited by* C. Mancuso, C. Jommi, and F. D'Onza. Springer-Verlag, Berlin Heidelberg. pp. 123–130. doi:10.1007/978-3-642-31116-1_16.

Al-Mukhtar, M., Belanteur, N., Tessier, D., and Vanapalli, S.K. 1996. The fabric of a clay soil under controlled mechanical and hydraulic stress states. Applied Clay Science, **11**: 99–115. doi:10.1016/S0169-1317(96)00023-3.

Alonso, E.E., Pinyol, N.M., and Puzrin, A.M. 2010. Collapse of compacted soil: Girona road embankments, Spain. *In* Geomechanics of failures. Advanced Topics, Springer. pp. 85–127.

Alonso, E., Pinyol, N., and Gens, A. 2013. Compacted soil behaviour: initial state, structure and constitutive modelling. Géotechnique, **63**(6): 463–478. doi:10.1680/geot.11.P.134.

ASTM. 2006. Standard practice for classification of soils for engineering purposes (unified soil classification system). ASTM standard D2487-06. ASTM. doi:10.1520/D2487-06.

Birle, E. 2012. Effect of initial water content and dry density on the pore structure and the soil-water retention curve of compacted clay. *In* Unsaturated soils: research and applications. *Edited by* C. Mancuso, C. Jommi, and F. D'Onza. Springer-Verlag, Berlin Heidelberg, pp. 145–152. doi:10.1007/978-3-642-31116-1_19.

Burland, J., Rampello, S., Georgiannou, V., and Calabresi, G. 1996. A laboratory study of the strength of four stiff clays. Géotechnique, **46**(3): 491–514. doi:10.1680/geot.1996.46.3.491.

Casagrande, A. 1936. The determination of the preconsolidation load and its practical significance. *In* Proceedings, First International Conference on Soil Mechanics, Cambridge. pp. 60–64.

Cotecchia, F., and Chandler, R.J. 1997. The influence of structure on the pre-failure behaviour of a natural clay. Géotechnique, **47**(3): 523–544. doi:10.1680/geot.1997.47.3.523.

Delage, P., and Lefebvre, G. 1984. Study of the structure of a sensitive Champlain clay and of its evolution during consolidation. Canadian Geotechnical Journal, **21**(1): 21–35. doi:10.1139/t84-003.

Delage, P., and Pellerin, M. 1984. Influence de la lyophilisation sur la structure d'une argile sensible du Québec. Clay Minerals, **19**: 151–160. doi:10.1180/claymin.1984.019.2.03.

Delage, P., Tessier, D., and Marcel-Audiguier, M. 1982. Use of the cryoscan apparatus for observation of freeze-fractured planes of a sensitive Quebec clay in scanning electron microscopy. Canadian Geotechnical Journal, **19**(1): 111–114. doi:10.1139/t82-011.

Delage, P., Audiguier, M., Cui, Y., and Howat, M.D. 1996. Microstructure of a compacted silt. Canadian Geotechnical Journal, **33**(1): 150–158. doi:10.1139/t96-030.

Graham, J., and Li, E. 1985. Comparison of natural and remolded plastic clay. Journal of Geotechnical Engineering, **111**(7): 865–881. doi:10.1061/(ASCE)0733-9410(1985)111:7(865).

Griffiths, F., and Joshi, R. 1989. Change in pore size distribution due to consolidation of clays. Géotechnique, **39**(1): 159–167. doi:10.1680/geot.1989.39.1.159.

Hammad, T., Fleureau, J.-M., and Hattab, M. 2013. Kaolin/montmorillonite mixtures behaviour on oedometric path and microstructural variations. European Journal of Environmental and Civil Engineering, **17**: 826–840. doi:10.1080/19648189.2013.822428.

Hattab, M., Hammad, T., Fleureau, J.-M., and Hicher, P.-Y. 2013. Behaviour of a sensitive marine sediment: microstructural investigation. Géotechnique, **63**(1): 71–84. doi:10.1680/geot.10.P.104.

Hattab, M., Hammad, T., and Fleureau, J.-M. 2015. Internal friction angle variation in a kaolin/montmorillonite clay mix and microstructural identification. Géotechnique, **65**(1): 1–11. doi:10.1680/geot.13.P.081.

Kochmanova, N., and Tanaka, H. 2011. Microstructure formation in bentonite. *In* Proceedings of the 17th International Conference on Soil Mechanics and Geotechnical Engineering. pp. 3392–3396.

Koliji, A., Lehmann, P., Vulliet, L., Laloui, L., Carminati, A., Vontobel, P., and Hassanein, R. 2008. Assessment of structural evolution of aggregated soil using neutron tomography. Water Resources Research, **44**: 2–9. doi:10.1029/2007WR006297.

Koliji, A., Vulliet, L., and Laloui, L. 2010. Structural characterization of unsaturated aggregated soil. Canadian Geotechnical Journal, **47**(3): 297–311. doi:10.1139/T09-089.

Lapierre, C., Leroueil, S., and Locat, J. 1990. Mercury intrusion and permeability of Louiseville clay. Canadian Geotechnical Journal, **27**(6): 761–773. doi:10.1139/t90-090.

Lawrence, G., Payne, D., and Greenland, D.J. 1979. Pore size distribution in critical point and freeze dried aggregates from clay subsoils. Journal of Soil Science, **30**(3): 499–516. doi:10.1111/j.1365-2389.1979.tb01004.x.

Leroueil, S., and Vaughan, R. 1990. The general and congruent effects of structure in natural soils and weak rocks. Géotechnique, **40**(3): 467–488. doi:10.1680/geot.1990.40.3.467.

Li, X., and Zhang, L.M. 2009. Characterization of dual-structure pore-size distribution of soil. Canadian Geotechnical Journal, **46**(2): 129–141. doi:10.1139/T08-110.

Liyanapathirana, D.S., Carter, J., and Airey, D.W. 2005. Numerical modeling of nonhomogeneous behavior of structured soils during triaxial tests. International Journal of Geomechanics, **5**(1): 10–23. doi:10.1061/(ASCE)1532-3641(2005)5:1(10).

Mitchell, J. 1976. Fundamentals of soil behavior. Wiley.

Monroy, R., Zdravkovic, L., and Ridley, A. 2007. Fabric changes in compacted london clay due to variations in applied stress and suction. *In* Experimental Unsaturated Soil Mechanics. Springer Proceedings in Physics, No. 112. pp. 41–48.

Monroy, R., Zdravkovic, L., and Ridley, A. 2010. Evolution of microstructure in compacted London clay during wetting and loading. Géotechnique, **60**(2): 105–119. doi:10.1680/geot.8.P.125.

Nowamooz, H., and Masrouri, F. 2010. Influence of suction cycles on the soil fabric of compacted swelling soil. Comptes Rendus Geoscience, **342**(12): 901–910. doi:10.1016/j.crte.2010.10.003.

Penumadu, D., and Dean, J. 2000. Compressibility effect in evaluating the pore-size distribution of kaolin clay using mercury intrusion porosimetry. Canadian Geotechnical Journal, **37**(2): 393–405. doi:10.1139/t99-121.

Romero, E., and Simms, P.H. 2008. Microstructure investigation in unsaturated soils: a review with special attention to contribution of mercury intrusion porosimetry and environmental scanning electron microscopy. Geotechnical and Geological Engineering, **26**(6): 705–727. doi:10.1007/s10706-008-9204-5.

Romero, E., Gens, A., and Lloret, A. 1999. Water permeability, water retention and microstructure of unsaturated compacted boom clay. Engineering Geology, **54**: 117–127. doi:10.1016/S0013-7952(99)00067-8.

Simms, P., and Yanful, E. 2002. Predicting soil-water characteristic curves of compacted plastic soils from measured pore-size distributions. Géotechnique, **52**(4): 269–278. doi:10.1680/geot.2002.52.4.269.

Sivakumar, V., Tan, W.C., Murray, E.J., and McKinley, J.D. 2006. Wetting, drying and compression characteristics of compacted clay. Géotechnique, **56**(1): 57–62. doi:10.1680/geot.2006.56.1.57.

Tarantino, A., and De Col, E. 2008. Compaction behaviour of clay. Géotechnique, **58**(3): 199–213. doi:10.1680/geot.2008.58.3.199.

Tessier, D., and Berrier, J. 1978. Observation d'argiles hydratées en microscopie electronique à balayage: Importance et choix de la technique de préparation. *In* Proceedings, Vth International Working-Meeting on Soil Micromorphology. Granada. pp. 117–135.

Thom, R., Sivakumar, R., Sivakumar, V., Murray, E.J., and Mackinnon, P. 2007. Pore size distribution of unsaturated compacted kaolin: the initial states and final states following saturation. Géotechnique, **57**(5): 469–474. doi:10.1680/geot.2007.57.5.469.

Tovey, D., and Wong, K. 1973. The preparation of soils and other geological materials for the S.E.M. *In* Proceedings of the International Symposium on Soil Structure, Gothenburg. pp. 59–67.

Watabe, Y., Leroueil, S., and Le Bihan, J.-P. 2000. Influence of compaction conditions on pore-size distribution and saturated hydraulic conductivity of a glacial till. Canadian Geotechnical Journal, **37**(6): 1184–1194. doi:10.1139/t00-053.

Yang, C., Carter, J.P., and Sheng, D. 2014. Description of compression behaviour of structured soils and its application. Canadian Geotechnical Journal, **51**(8): 921–933. doi:10.1139/cgj-2013-0265.